Cherenkov Radiation from Photonic Bound States in the Continuum: Towards Compact Free-Electron Lasers

Yanan Song,[1] Ningxiao Jiang,[1] Liu Liu,[1] Xinhua Hu,[1,*] and Jian Zi[2,†]

[1] *Department of Materials Science, Key Laboratory of Micro- and Nano-Photonic Structures (Ministry of Education), and Laboratory of Advanced Materials, Fudan University, Shanghai 200433, China*

[2] *Department of Physics, State Key Laboratory of Surface Physics, and Collaborative Innovation Center of Advanced Microstructures, Fudan University, Shanghai 200433, China*

(Received 1 June 2018; revised manuscript received 20 November 2018; published 11 December 2018)

In conventional materials, Cherenkov radiation (CR) due to a moving charged particle is associated with a broad frequency range and velocity threshold. Here, we show that using a periodic grating structure, which possesses photonic bound states in the continuum (BICs) and quasi-BICs, unusual CR can be generated in a very narrow frequency band at a particle velocity below the common threshold. This effect arises from an interesting light-amplification process in the BIC structure, which can dramatically improve the efficiencies of evanescent-to-propagating wave conversion and CR generation. Our results present a mechanism for realizing Cherenkov lasing at low electron velocity and may find applications in compact free-electron lasers.

DOI: 10.1103/PhysRevApplied.10.064026

I. INTRODUCTION

When a charged particle moves in a medium, it can drive the medium to emit coherent propagating electromagnetic (EM) waves. Such a phenomenon, first experimentally discovered by Cherenkov [1] and now called Cherenkov radiation (CR), has been widely used in particle detectors and counters and forms the basis of free-electron light sources [2].

In conventional materials, CR occurs only when the particle velocity exceeds the medium's phase velocity [2]. If the particle velocity is below the velocity threshold, only evanescent waves can be detected in the vicinity of the moving particle. In 1953, Smith and Purcell experimentally demonstrate that using a diffraction grating, the evanescent waves of moving particles can be converted into propagating waves [3]. As it works without any velocity threshold, such a new type of CR presents a possibility in the development of compact free-electron light sources (which do not require a high electron velocity and large electron accelerator). However, such unusual CR still exhibits characteristics of a low evanescent-to-propagating wave conversion efficiency and wide frequency range. Hence, it remains difficult to construct compact free-electron lasers [4]. Although considerable efforts have been devoted to study CR in more complex artificial structures such as photonic crystals (PCs) and metamaterials [5–19], this problem remains unsolved.

In this paper, we investigate CR in a new class of photonic structure, which possesses photonic bound states in the continuum (BICs) and quasi-BICs. BIC is initially a concept in quantum mechanics, which refers to an unusual bound state with energy above the continuum threshold [20–22]. Recently, BIC has been realized essentially as a wave phenomenon and its photonic analog has been created in certain periodic photonic structures [23–40]. Such photonic BICs manifest themselves as modes with the infinite quality (Q) factor above the light line (i.e., in the continuum of free-space modes). When the photonic BICs and quasi-BICs are excited, a very strong field can occur in a large area of structure, enabling many fascinating phenomena and applications [23–40]. While photonic BIC structures have been extensively investigated, their abilities of evanescent-to-propagating wave conversion and CR generation have seldom been studied.

Here, we focus on a photonic BIC structure consisting of two parallel equivalent dielectric gratings [23–25]. By adjusting the distance between the two gratings, the Q factor of the structure can be flexibly tuned, resulting in photonic BICs and quasi-BICs. It is found that the wave conversion efficiency at resonant frequency can increase linearly with increasing the Q factor of the BIC structure, much higher than those in common diffraction gratings. Based on this effect, strong CR can be, in principle, realized in a very narrow frequency range, leading to Cherenkov lasing at a relatively low particle velocity. Our results arise from an interesting light-amplification process in the double-grating structure, and can be anticipated in other BIC structures.

*huxh@fudan.edu.cn
†jzi@fudan.edu.cn

II. RESULTS

The structures under study are a single grating and a double grating that are located in the vacuum, as shown in Fig. 1. The structures have a period p in the x direction and is invariant in the y direction. The upper surfaces of the structures are at $z = 0$. The gratings are composed of dielectric strips with a width $w_1 = 0.6p$, thickness $w_2 = 0.4p$, and refractive index $n = 3.44$. Here, $n = 3.44$ corresponds to Si at $\lambda = 2.5$ μm. Since the refractive index of Si changes slightly in the infrared region ($3.49 > n > 3.42$ for λ from 1.4 to 333 μm) [41], our results can be valid in a wide frequency range by using different period p (but nearly unchanged ratios of λ/p, w_1/p, and w_2/p). Hence, we will show our results as a function of the ratio p/λ or the normalized frequency $fp/c \equiv p/\lambda$, where f is the frequency, and c and λ are the light velocity and wavelength in the vacuum, respectively. For the case of evanescent wave incidence, the wave conversion efficiencies can be defined as $C_r = |c_r|^2 = |H_3/H_1|^2$ and $C_t = |c_t|^2 = |H_4/H_1|^2$. Here, the incident evanescent wave and outgoing propagating waves have wavevectors in the x-z plane and H field along the y direction. H_1 is the H field of incident evanescent wave at the upper surface of the grating, and H_3 and H_4 are the H field of the upward and downward propagating waves, respectively. The incident evanescent wave and outgoing propagating waves possess a parallel component of wavevector k_x and $k_x - 2\pi/p$, respectively. We also study the case of normal incidence of propagating waves with H field in the y direction. All the simulations are conducted by using a commercial finite-element software of COMSOL MULTIPHYSICS.

We first discuss the single-grating structure. In Fig. 1(a), the specular reflection coefficient $R_0 = |r_0|^2$ is plotted as a function of the normalized frequency $fp/c \equiv p/\lambda$ for normal incidence of a propagating plane wave. A low-Q resonance ($Q_0 = 3.0$) is visible at normalized frequency $f_{R0}p/c = 0.48825$. At the resonance, total reflection occurs [24,25] and the field is concentrated at the dielectric strips. Due to the diffraction effect, the single grating can also convert an incident evanescent plane wave into outgoing propagating plane waves. The corresponding wave conversion efficiencies of $C_{r0} = |c_{r0}|^2$ and $C_{t0} = |c_{t0}|^2$ are shown in Fig. 1(b), where the incident evanescent wave and outgoing propagating waves possess a parallel component of wavevector $k_x = 2\pi/p$ and $k_x = 0$, respectively. Moderate wave conversion efficiencies ($C_{r0} < 0.6$, $C_{t0} < 0.15$) can be seen in a broad range of frequency.

We study a double-grating structure composed of two equivalent dielectric gratings. The distance between the two gratings is $h = 0.23p$, and the other parameters are the same as those of the above single dielectric grating. In Fig. 1(c), the specular reflection spectrum is shown for normal incidence of propagating plane waves. A high-Q resonance ($Q = 6504$) can be seen at

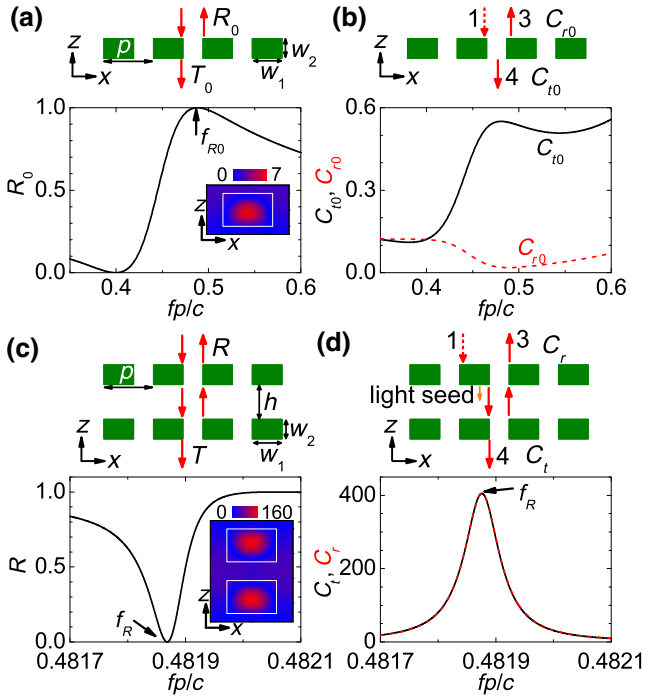

FIG. 1. (a) Top panel: schematic of the normal impinging of a propagating plane wave upon a single dielectric grating. The grating has a period of p along the x direction and is invariant in the y direction. The dielectric strips in the gratings have a width w_1, thickness w_2, and refractive index n. Bottom panel: specular reflection coefficient R as a function of normalized frequency $fp/c \equiv p/\lambda$. Inset: the profile of $|H_y(x,z)|$ at resonant frequency, where the incident propagating plane wave has $|H_y| = 1$ and the white rectangles outline the dielectric strips. (b) Top panel: schematic of the impinging of an evanescent plane wave upon the single grating. The incident evanescent plane wave has a parallel component of wavevector k_x and can be converted into outgoing propagating waves with a parallel component of wavevector $k_x - 2\pi/p$. Bottom panel: wave conversion efficiencies, C_r and C_t, for $k_x = 2\pi/p$. (c),(d) The same as (a),(b) but for a double dielectric grating. The distance between the two gratings $h = 0.23p$. In (a)–(d), all the gratings have the same parameters: $n = 3.44$ (corresponding to Si at $\lambda = 2.5$ μm), $w_1 = 0.6p$, and $w_2 = 0.4p$.

normalized frequency $f_R p/c \equiv p/\lambda_R = 0.48188$, where λ_R is the resonant wavelength in the vacuum. Due to the resonance tunneling effect, total transmission is observed at the resonant frequency. Compared with the case of single grating, much stronger field can be excited in the double-grating structure [24]. Such a strong resonance can be called quasi-BIC [23,24]. In Fig. 1(d), the wave conversion efficiencies are then demonstrated for the double grating. Very efficient wave conversion ($C_t = 405.2$, $C_r = 405.9$) can be seen at the resonant frequency, much more efficient than that ($C_{t0} = 0.55$, $C_{r0} = 0.08$) in the single grating.

To qualitatively understand the physics behind the above simulated results, we consider a simplified model for the double-grating structure. In the region between

the two gratings, only propagating waves are considered while the evanescent waves are neglected. The constituent single grating is regarded as a resonator array with transmission amplitude $t_0(\omega)$, reflection amplitude $r_0(\omega)$, and wave conversion efficiencies $c_{r0}(\omega)$ and $c_{t0}(\omega)$, where $\omega = 2\pi f$ is the angular frequency. In the vicinity of the resonant angular frequency $\omega_{R0} = 2\pi f_{R0}$, the transmission and reflection amplitude can be approximated by the Breit-Wigner form [24]:

$$t_0 = \frac{(\omega - \omega_{R0})\exp(i\varphi_{t0})}{\omega - \omega_{R0} + i\Gamma_0/2}, \quad r_0 = \frac{i(\Gamma_0/2)\exp(i\varphi_{r0})}{\omega - \omega_{R0} + i\Gamma_0/2}, \tag{1}$$

where $\Gamma_0 = \omega_{R0}/Q_0$ is the width of the resonance. The reflection phase φ_{r0} is a function of frequency, and $\varphi_{r0} \approx \varphi_{r0}(\omega_{R0}) + a_1(\omega_R - \omega_{R0})$ near the resonance. Based on a Fabry-Perot-type approach (or a 2×2 transfer matrix method) [24,42,43], the transmission amplitude and wave conversion efficiencies of the double grating can be obtained:

$$t = \frac{t_0^2}{g^{-1} - gr_0^2}, \quad c_t = \frac{c_{t0}t_0}{g^{-1} - gr_0^2}, \quad c_r = c_{r0} + c_t g r_0, \tag{2}$$

where $g = e^{ik_z h}$, $k_z = \sqrt{k_0^2 - k_{xp}^2}$, $k_0 = \omega/c$ is the wavenumber in the vacuum, k_{xp} is the parallel component of the wavevector for the propagating plane waves between the two gratings, and $k_{xp} = k_x$ ($k_{xp} = k_x - 2\pi/p$) for the incidence of propagating (evanescent) plane wave. By considering the pole of the transmission t [24,43], two resonances can be found for the double grating and their frequencies and widths are given by

$$\omega_R = \omega_{R0} \pm \Gamma_0 \sin(k_z h)/2, \quad \Gamma = \Gamma_0[1 \pm \cos(k_z h)]. \tag{3}$$

When $k_z h = m\pi$ with m being an integer, the two resonances have the same resonant frequency ($\omega_R = \omega_{R0}$) but different width. One resonance has a vanishing width forming a BIC ($\Gamma = 0$), whereas the other acquires the double width ($\Gamma = 2\Gamma_0$) [24,43]. For the case of $k_{xp} = 0$, the BIC occurs when the distance between the two gratings is $h_0 \approx m\pi c/\omega_{R0}$. For a distance h close to h_0, we have

$$\omega_R \approx \omega_{R0}[1 - a_2\omega_{R0}(h - h_0)/c], \tag{4}$$

$$Q \approx \frac{\omega_{R0}^2}{2Q_0(\omega_R - \omega_{R0})^2}, \tag{5}$$

$$C_r \approx C_t \approx C_{t0}Q/(2Q_0), \tag{6}$$

where $a_2 = [2Q_0 + \omega_{R0}(a_1 + h_0/c)]^{-1}$, and C_r, C_t, and C_{t0} are the conversion efficiencies at the resonant frequency ω_R.

From the above formulas, we can see that for the incidence of evanescent plane waves, the double-grating structure can provide more efficient wave conversion ($C_t/C_{t0} \approx Q/(2Q_0) \gg 1$) at the resonant frequency. We note that when the evanescent plane wave is incident on the double-grating structure, a propagating plane wave with amplitude $c_{t0}H_1$ will be first produced under the upper grating and then bounce back and forth multiple times between the two gratings. At the BIC point, the multiple reflected propagating waves can constructively interfere, leading to very strong field in the cavity. Consequently, strong outgoing propagating waves can be observed from the system. In other words, the initial propagation wave generated by the upper grating serves as a light seed [shown as the orange arrow in the inest to Fig. 1(d)], which can be amplified by the Fabry-Perot cavity [see Fig. S1(b) in the Supplemental Material]. The light-amplification process can become very efficient at the BIC, resulting in a lasinglike output.

To check the validity of the above formulas, more simulations are performed for the BIC structure with different distance h [see Fig. 2]. As the ratio h/p increases from 0.2 to 0.23, the resonant frequency decreases slightly [Fig. 2(a)]. In contrast, the Q factor and wave conversion efficiency of the structure change dramatically [Fig. 2(b)]. At $h = h_0 = 0.21437p$, very large values can be seen for both the Q factor and wave conversion efficiency. It is also found that the wave conversion efficiency can increase linearly with increasing the Q factor ($C_r = 0.06504Q$). These simulated results can be well described by the above model. By fitting the curves in Figs. 2(b) and 2(c) with Eqs. (5) and (6), we can obtain the fitting parameters of $Q_0 = 2.96$ and $C_{t0} = 0.385$. We note that in our model,

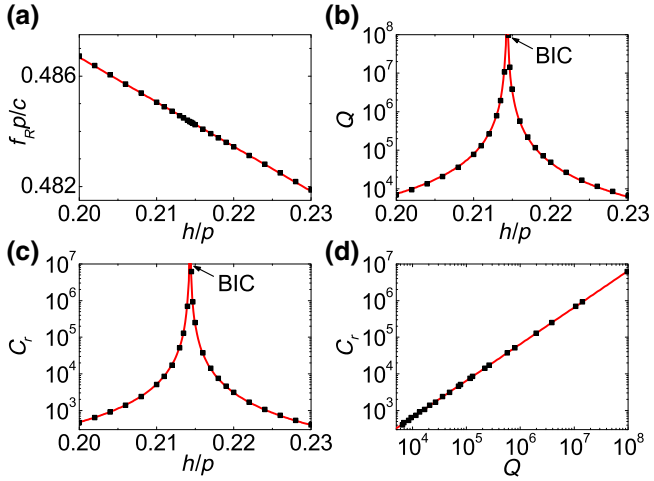

FIG. 2. (a) Normalized resonant frequency $f_R p/c \equiv p/\lambda_R$, (b) Q factor, and (c) wave conversion efficiency C_r at f_R as a function of the distance h for the peak in Fig. 1(d). (d) Wave conversion efficiency C_r at f_R as a function of the Q factor. Dots are simulated results. Red curves are obtained from Eqs. (4)–(6) with appropriate fitting parameters.

only the first wave conversion at the upper grating is considered and other wave conversion processes are neglected. Hence, the fitting parameters here are slightly different from the values ($Q_0 = 3.0$, $C_{t0} = 0.550$) in Figs. 1(a) and 1(b).

The above studies have been focused on incident evanescent plane waves with parallel component of wavevector $k_x = 2\pi/p$. In Fig. 3, more results are presented for different values of k_x. When $|k_x - 2\pi/p| < k_0$, the incident evanescent plane wave can be converted into outgoing propagating plane waves [i.e., in the white region in Figs. 3(a), 3(d), and 3(h)]. Maximal conversion efficiencies can be achieved when the incident evanescent wave has a frequency f_R (k_x) as shown in Figs. 3(a), 3(d), and 3(h). Here, the resonant frequency varies a little (< 20%) for different k_x. Correspondingly, the Q factors are also shown in Figs. 3(b), 3(e), and 3(i). When $h > h_0$, two BICs can be seen [Fig. 3(i)]. As $h = h_0$, the two BICs become degenerate at $k_x = 2\pi/p$ [Fig. 3(e)]. When $h < h_0$, no BICs can be observed in Fig. 3(b). In fact, the number of BICs is conserved [31]. To observe BICs for $h < h_0$, the incident evanescent waves need to possess $k_x = 2\pi/p$ and nonzero k_y. Because of the large Q factor, a high wave conversion efficiency C_r is also observed [Figs. 3(c), 3(f), and 3(j)]. For $h > h_0$, very efficient wave conversion can be achieved when the BICs are excited.

Based on the efficient evanescent-to-propagating wave conversion, unusual CR can be observed in the BIC structures. Here, we consider an electron bunch that has a line charge density q along the y direction and moves at $z = b$ with a velocity v along the x direction. The electron bunch can generate evanescent plane waves with wavevectors $(k_x, -i\gamma)$ in the x-z plane and H field of $H_1 \exp(\gamma z + ik_x x - i\omega \mathrm{t})$ (for $z < b$) in the y direction [16,17]. Here, t is time, $H_1 = I_0 e^{-\gamma b}/2$, $I_0 = q/(2\pi)$, $\gamma = \sqrt{k_x^2 - k_0^2}$, $k_x = \omega/v$ [as shown as the dashed line in Fig. 3(h)], and the angular frequency ω varies from 0 to infinity. It can be seen that the CR generated by the double dielectric grating exhibits high intensity as well as narrow ranges in both emission angle and frequency [Figs. 4(d), 4(e), and 4(f); $|E_{\max}| = 1260$ V/m here, much higher than $|E_{\max}| = 79$ V/m in [16]], which are unachievable by corresponding single grating [Figs. 4(a), 4(b), and 4(c)]. Here, besides the emission angle and central frequency f_R, both the E-field amplitude at f_R and width ($\Delta_f = f_R/Q$) of the CR also depend on the electron velocity [Fig. 5]. At certain electron velocities, BICs can be excited resulting in infinitely narrow width and very high intensity for the CR [Figs. 5(c) and 5(d); we note that the maximal intensity $|E| = 79$ V/m in [16]]. Since the CR peak possesses a height inversely proportional to its width, the total radiation power remains finite at BICs. We remark that traditional free-electron lasers work at an electron velocity very close to the light speed in the vacuum ($v \approx 0.999c$) [4], requiring large and complex electron accelerators. In contrast, only a low electron velocity ($v = 0.48c$) is needed in our design [Fig. 4(e); the lowest electron velocity $v_{\min} \approx c/n$ for the dielectric BIC systems and $v_{\min} \approx 0.29c$ for $n = 3.44$], facilitating the realization of compact free-electron lasers.

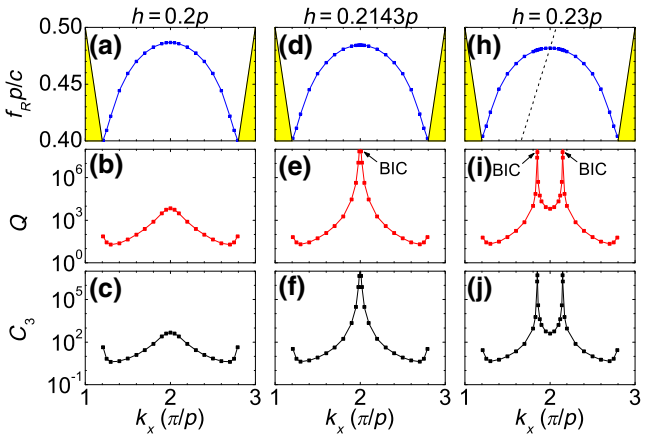

FIG. 3. (a) Normalized resonant frequency $f_R p/c \equiv p/\lambda_R$, (b) Q factor, and (c) wave conversion efficiency C_r at f_R for the impinging of an evanescent plane wave with parallel component of wavevector k_x upon a double dielectric grating with $h = p/5$, $w_1 = 0.6p$, $w_2 = 0.4p$, and $n = 3.44$. (d)–(f) The same as (a)–(c) but for $h = 0.2143p$. (h)–(j) The same as (a)–(c) but for $h = 0.23p$.

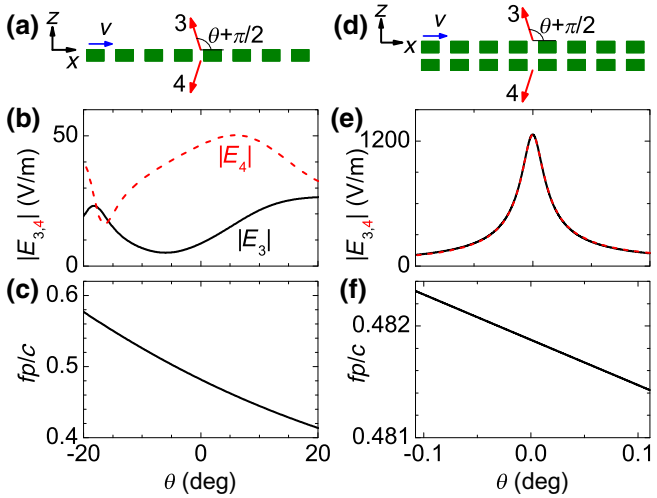

FIG. 4. (a) Schematic of a charged particle moving close and parallel to the surface of a single grating. An upgoing (downgoing) EM wave 3 (4) with an E field E_3 (E_4) can be produced at angle θ. The charged particle has parameters of $v = 0.48188c$, $I_0 = 1$ A/m, and $b = p/5$. The grating parameters are the same as in Fig. 1(b). (b) E-field amplitude $|E_{3,4}|$ and (c) normalized frequency $fp/c \equiv p/\lambda$ of outgoing EM waves at different angle θ. (d)–(f) The same as (a)–(c) but for the double dielectric grating in Fig. 1(d).

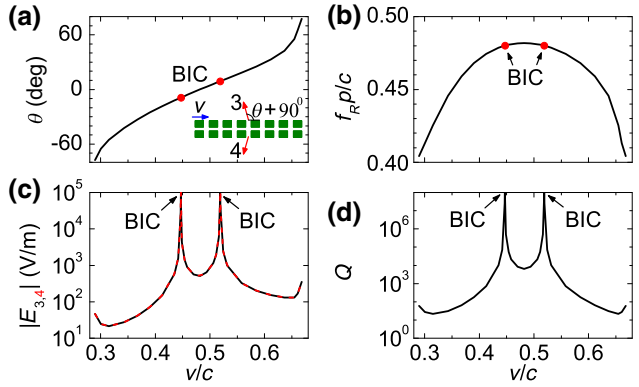

FIG. 5. (a) Emission angle, (b) normalized peak frequency $f_R p/c \equiv p/\lambda_R$, (c) E-field amplitude of CR $|E_{3,4}|$ at f_R, and (d) Q factor for the radiation peak in Fig. 4(e). Except the particle velocity v, the other parameters are the same as those in Fig. 4(e).

Finally, we remark that the above results are based on a dielectric double grating and can be anticipated in other Fabry-Perot BIC structures. To construct such BIC structures, a dielectric or vacuum layer needs to be sandwiched between two reflecting mirrors with periodic structures [24–26]. Here, the mirrors are required to not only convert incident evanescent plane waves into outgoing propagating waves but also highly reflect propagating plane waves at resonant frequency. Besides the above one-dimensional dielectric grating [24], two-dimensional dielectric PC slabs can also serve as the reflecting mirrors (see Fig. S2 in the Supplemental Material) [25,43]. In addition, a thick dielectric grating can also be a BIC system (see Fig. S4 in the Supplemental Material) [31,43]. For such dielectric BIC structures, some realistic factors such as surface roughness, the introduction of a substrate, and a finite sample size can lower the Q factor of the structure [35,36]. However, through a good design and fine fabrication, a high Q factor (80 000) can still be achieved in experiments [28,34]. Such quasi-BIC structures with high Q factors will exhibit high efficiencies for wave conversion and CR generation at resonant frequency [see Figs. S2 and S4 in the Supplemental Material]. Moreover, metallic metasurfaces can also serve as the reflecting mirrors [16,43], which can have much smaller thickness than dielectric gratings and PC slabs. But due to the Joule loss of metal, a relatively low Q factor and wave conversion efficiency may occur in the metallic structures [see Fig. S3 in the Supplemental Material].

III. SUMMARY

In summary, we demonstrate that using a periodic grating structure, which supports photonic BICs and quasi-BICs, very efficient evanescent-to-propagating wave conversion can be achieved at resonant frequency. This effect arises from an interesting light-amplification process in the Fabry-Perot BIC structure. As a result, strong CR can be produced at a narrow frequency region at a relatively low particle velocity. Our results present a mechanism for realizing Cherenkov lasing at low electron velocity and may benefit the construction of compact free-electron lasers.

ACKNOWLEDGMENTS

This work was supported by the National Key R&D Program of China (Grant No. 2018YFA0306201) and the NSFC (Grants No. 61422504, No. 11574037, and No. 11604355).

[1] P. A. Cerenkov, Visible emission of clean liquids by action of gamma radiation, Dokl. Akad. Nauk SSSR **2**, 451 (1934).
[2] J. V. Jelley, *Cerenkov Radiation and its Applications* (Pergamon, London, 1958).
[3] S. J. Smith, and E. M. Purcell, Visible light from localized surface charges moving across a grating, Phys. Rev. **92**, 1069 (1953).
[4] P. G. O'Shea, and H. P. Freund, Free-electron lasers: Status and applications, Science **292**, 1853 (2001).
[5] F. J. Garcia de Abajo, Interaction of Radiation and Fast Electrons with Clusters of Dielectrics: A Multiple Scattering Approach, Phys. Rev. Lett. **82**, 2776 (1999).
[6] S. Yamaguti, J. I. Inoue, O. Haeberlé, and K. Ohtaka, Photonic crystals versus diffraction gratings in Smith-Purcell radiation, Phys. Rev. B **66**, 195202 (2002).
[7] C. Luo, M. Ibanescu, S. G. Johnson, and J. Joannopoulos, Cerenkov radiation in photonic crystals, Science **299**, 368 (2003).
[8] S. Xi, H. Chen, T. Jiang, L. Ran, J. Huangfu, B.-I. Wu, J. A. Kong, and M. Chen, Experimental Verification of Reversed Cherenkov Radiation in Left-Handed Metamaterial, Phys. Rev. Lett. **103**, 194801 (2009).
[9] G. Adamo, K. F. MacDonald, Y. H. Fu, C-M. Wang, D. P. Tsai, F. J. Garcia de Abajo, and N. I. Zheludev, Lightwell: A Tunable Free-Electron Light Source on a Chip, Phys. Rev. Lett. **103**, 113901 (2009).
[10] F. J. Garcia de Abajo, Optical excitations in electron microscopy, Rev. Mod. Phys. **82**, 209 (2010).
[11] D. E. Fernandes, S. I. Maslovski, and M. G. Silveirinha, Cherenkov emission in a nanowire material, Phys. Rev. B **85**, 155107 (2012).
[12] V. V. Vorobev, and A. V. Tyukhtin, Nondivergent Cherenkov Radiation in a Wire Metamaterial, Phys. Rev. Lett. **108**, 184801 (2012).
[13] T. Zhan, D. Han, X. Hu, X. Liu, S. T. Chui, and J. Zi, Tunable terahertz radiation from graphene induced by moving electrons, Phys. Rev. B **89**, 245434 (2014).
[14] T. Denis, M. W. van Dijk, J. H. H. Lee, R. van der Meer, A. Strooisma, P. J. M. van der Slot, W. L. Vos, and K.-J. Boller, Coherent Cherenkov radiation and laser oscillation in a photonic crystal, Phys. Rev. A **94**, 053852 (2016).
[15] J. S. Hummelt, X. Lu, H. Xu, I. Mastovsky, M. A. Shapiro, and R. J. Temkin, Coherent Cherenkov-Cyclotron Radiation Excited by an Electron Beam in a Metamaterial Waveguide, Phys. Rev. Lett. **117**, 237701 (2016).

[16] Z. Wang, K. Yao, M. Chen, H. Chen, and Y. Liu, Manipulating Smith-Purcell Emission with Babinet Metasurfaces, Phys. Rev. Lett. **117**, 157401 (2016).
[17] L. Liu, H. Chang, C. Zhang, Y. Song, and X. Hu, Terahertz and infrared Smith-Purcell radiation from Babinet metasurfaces: Loss and efficiency, Phys. Rev. B **96**, 165435 (2017).
[18] F. Liu, L. Xiao, Y. Ye, M. Wang, K. Cui, X. Feng, W. Zhang, and Y. Huang, Integrated Cherenkov radiation emitter eliminating the electron velocity threshold, Nature Photon. **11**, 289 (2017).
[19] Y. Song, J. Du, N. Jiang, L. Liu, and X. Hu, Efficient terahertz and infrared Smith-Purcell radiation from metal-slot metasurfaces, Opt. Lett. **43**, 3858 (2018).
[20] J. von Neuman, and E. Wigner, Über merkwürdige diskrete Eigenwerte, Phys. Z. **30**, 465 (1929).
[21] H. Feshbach, Unified theory of nuclear reactions, Ann. Phys. **5**, 357 (1958).
[22] H. Friedrich, and D. Wintgen, Interfering resonances and bound states in the continuum, Phys. Rev. A **32**, 3231 (1985).
[23] C. W. Hsu, B. Zhen, A. D. Stone, J. D. Joannopoulos, and M. Soljačić, Bound states in the continuum, Nat. Rev. Mater. **1**, 16048 (2016).
[24] D. C. Marinica, A. G. Borisov, and S. V. Shabanov, Bound States in the Continuum in Photonics, Phys. Rev. Lett. **100**, 183902 (2008).
[25] W. Suh, M. F. Yanik, O. Solgaard, and S. Fan, Displacement-sensitive photonic crystal structures based on guided resonance in photonic crystal slabs, Appl. Phys. Lett. **82**, 1999 (2003).
[26] C. W. Hsu, B. Zhen, S.-L. Chua, S. G. Johnson, J. D. Joannopoulos, and Marin Soljačić, Bloch surface eigenstates within the radiation continuum, Light: Sci. Appl. **2**, e84 (2013).
[27] Y. Plotnik, O. Peleg, F. Dreisow, M. Heinrich, S. Nolte, A. Szameit, and M. Segev, Experimental Observation of Optical Bound States in the Continuum, Phys. Rev. Lett. **107**, 183901 (2011).
[28] C. W. Hsu, B. Zhen, J. Lee, S.-L. Chua, S. G. Johnson, J. D. Joannopoulos, and M. Soljačić, Observation of trapped light within the radiation continuum, Nature **499**, 188 (2013).
[29] S. Weimann, Y. Xu, R. Keil, A. E. Miroshnichenko, A. Tünnermann, S. Nolte, A. A. Sukhorukov, A. Szameit, and Y. S. Kivshar, Compact Surface Fano States Embedded in the Continuum of Waveguide Arrays, Phys. Rev. Lett. **111**, 240403 (2013).
[30] Y. Yang, C. Peng, Y. Liang, Z. Li, and S. Noda, Analytical Perspective for Bound States in the Continuum in Photonic Crystal Slabs, Phys. Rev. Lett. **113**, 037401 (2014).
[31] B. Zhen, C. W. Hsu, L. Lu, A. D. Stone, and M. Soljačić, Topological Nature of Optical Bound States in the Continuum, Phys. Rev. Lett. **113**, 257401 (2014).
[32] E. N. Bulgakov, and D. N. Maksimov, Topological Bound States in the Continuum in Arrays of Dielectric Spheres, Phys. Rev. Lett. **118**, 267401 (2017).
[33] Y. Guo, M. Xiao, and S. Fan, Topologically Protected Complete Polarization Conversion, Phys. Rev. Lett. **119**, 167401 (2017).
[34] A. Kodigala, T. Lepetit, Q. Gu, B. Bahari, Y. Fainman, and B. Kanté, Lasing action from photonic bound states in continuum, Nature **541**, 196 (2017).
[35] Z. F. Sadrieva, I. S. Sinev, K. L. Koshelev, A. Samusev, I. V. Iorsh, O. Takayama, R. Malureanu, A. A. Bogdanov, and A. V. Lavrinenko, Transition from optical bound states in the continuum to leaky resonances: Role of substrate and roughness, ACS Photon. **4**, 723 (2017).
[36] E. N. Bulgakov, and D. N. Maksimov, Light enhancement by quasi-bound states in the continuum in dielectric arrays, Opt. Exp. **25**, 14134 (2017).
[37] J. Gomis-Bresco, D. Artigas, and L. Torner, Anisotropy-induced photonic bound states in the continuum, Nature Photon. **4**, 232 (2017).
[38] Y. Zhang, A. Chen, W. Liu, C. W. Hsu, B. Wang, F. Guan, X. Liu, L. Shi, L. Lu, and J. Zi, Observation of Polarization Vortices in Momentum Space, Phys. Rev. Lett. **120**, 186103 (2018).
[39] V. A. Fedotov, M. Rose, S. L. Prosvirnin, N. Papasimakis, and N. I. Zheludev, Sharp Trapped-Mode Resonances in Planar Metamaterials with a Broken Structural Symmetry, Phys. Rev. Lett. **99**, 147401 (2007).
[40] R. Singh, I. A. I. Al-Naib, Y. Yang, D. R. Chowdhury, W. Cao, C. Rockstuh, T. Ozaki, R. Morandotti, and W. Zhang, Observing metamaterial induced transparency in individual Fano resonators with broken symmetry, Appl. Phys. Lett. **99**, 201107 (2011).
[41] E. D. Palik, ed. *Handbook of Optical Constants of Solids* (Academic, Orlando, 1985).
[42] J. Zi, J. Wan, and C. Zhang, Large frequency range of negligible transmission in one-dimensional photonic quantum well structures, Appl. Phys. Lett. **73**, 2084 (1998).
[43] See Supplemental Material at http://link.aps.org/supplemental/10.1103/PhysRevApplied.10.064026 for the derivation of Eqs. (2)–(6) and more information about the studies.